Electronic Supplementary Material (ESI) for Chemical Communications.

Concerted effect of Ni-in and S-out on ReS_2 nanostructures towards high-efficiency oxygen evolution reaction

Tapas K. Das,[a] Tapan Ping,[a,b] Manoj Mohapatra,[c,d] Shahid Anwar,[a] Chinnakonda S. Gopinath[e] and Bikash Kumar Jena,*[a,b]

[a]Materials Chemistry Department, CSIR-Institute of Minerals and Materials Technology, Bhubaneswar, Odisha, 751013, India

[b]Academy of Scientific & Innovative Research, Ghaziabad-201002, India

[c]Radiochemistry Division, Bhabha Atomic Research Centre, Trombay, Mumbai-400085, India

[d] Homi Bhabha National Institute, Anushakti Nagar, Mumbai-400094

[e]Catalysis and Inorganic Chemistry Division, CSIR-National Chemical Laboratory, Dr. Homi Bhabha Road, Pune-411008, India

*Email: bikash@immt.res.in

Experimental Section:

Chemicals and Reagents:

Ammonium perrhenate (NH_4ReO_4, 99.99%) and 5% Nafion from Sigma Aldrich, Ruthenium oxide (RuO_2, 99.9%) from Alfa Aesar, Nickel nitrate hexahydrate ($Ni(NO_3)_2.6H_2O$), Thio-Urea($CS(NH_2)_2$, Hydrazine Hydrate($(NH_2)_2.H_2O$) (25%), sodium tetrahydridoborate ($NaBH_4$) were purchased from HiMedia chemicals. All the chemicals used in this work are as received with analytical grade. All the solution was prepared using the deionized water (18.2 MΩ) obtained by the Millipore milli-Q water purification system.

Synthesis of Ni doped ReS_2: $Ni_d(5)@ReS_2$ NS, $Ni_d(1)@ReS_2$ NS and $Ni_d(10)@ReS_2$ NS

$Ni_d(5)@ReS_2$ was synthesized by a simple single one-step hydrothermal method. In detail, 1 mmol of NH_4ReO_4, 0.05 mmol of $Ni(NO_3)_2.6H_2O$, 8 mmol of $CS(NH_2)_2$ were mixed in 30 ml of deionized water. Then 6 ml of Hydrazine hydrate was added slowly to the mixture and further mixed for half an hour. Then the resulting mixture was transferred into a 100 ml Teflon-lined stainless-steel autoclave. The autoclave was heated at 220 °C for 24 hours inside a hot air oven, and then it was cooled down to room temperature naturally. The as-synthesized black color

materials were centrifuged at 10000 rpm for 15 minutes and washed with water and methanol and dried in a vacuum oven, and kept in a desiccator for prior use, and the materials were named $Ni_d(5)@ReS_2$ NS. Similarly, 1% and 10 % Ni doped ReS_2 were prepared by following the same method by changing the concentration of $Ni(NO_3)_2.6H_2O$ and are referred to as $Ni_d(1)@ReS_2$ NS and $Ni_d(10)@ReS_2$ NS, respectively. Also, the ReS_2 NS was prepared following the same procedure as above without adding Ni precursor.

Synthesis of $Ni_d(5)S_v@ReS_2$ NS:

20 mg of the as-synthesized $Ni_d(5)@ReS_2$ NS was dispersed in 8 ml of deionized water and sonicated for 30 min. Then, 0.80 mg of $NaBH_4$ was added to it, and the stirring was continued for different times 10 min, 20 min, 30 min, and 60 min. After that, the solution was centrifuged and washed with water and methanol at 1100 rpm. The samples were dried at 60 °C in a vacuum oven and kept in a desiccator for prior use. The samples were labeled as the $Ni_d(5)S_v@ReS_2$ NS-x min, where x stands for the different times of chemical treatments, 10, 20, 30, and 60 min.

Synthesis of IrO_2/C:

The IrO_2/C colloidal was prepared by using our previously reported process.[1,2] Briefly, 100 mg potassium hexachloroirridate (K_2IrCl_6) was mixed in a 50 ml aqueous solution of sodium hydrogen citrate sesquihydrate (0. 63 mM). The pH of the solutions was adjusted to 7.5 by heating and the addition of NaOH. Then, 0.184 g of carbon nanopowder was added to the solutions and ultrasonicated for 1 hr to get a high dispersion. After that, the solution was further heated at 95 °C for 2 hours in the O_2 environment. The sample was dried at 60 °C in a vacuum oven for 6 hours. The sample was heated at 300 °C for 30 minutes in the Ar environment to remove any remaining organic contaminant.

Characterization:

Powered X-ray diffraction patterns were recorded on X'pert PRO (Pan Analytical) X-ray diffraction unit using Ni filtered Cu Kα (λ = 1.54 Å) radiation at 40kV over a 2θ range of 10°- 70°. Structural and morphological analysis of the as-synthesized samples were carried out by using a scanning electron microscope (SEM, Zeiss EVO18) with a 20 keV electron gun. High-resolution Transmission electron microscope (HR-TEM) images were obtained using JEM F200 200 kV (make JEOL Japan) electron microscope. The TEM samples were prepared by fine dispersion of the sample in ethanol and drop casted on carbon-coated copper grids and were dried under the

Lamp of 100W prior to analysis. X-ray photoelectron spectra (XPS) were carried out on VG Microtech Multilab ESCA 3000 spectrometer equipped with non-monochromatized Al Kα (1486.6 eV) or Mg Kα(1253.6 eV) x-ray sources. The high-resolution spectra were deconvoluted using the Gaussian function. EPR spectrum of all sample recorded at X band frequency (9.5 GHz) at room temperature using Bruker (EMM1843) spectrometer.

Sample preparation for electrochemical study:

The glassy carbon (GC) electrode (geometric surface area of 0.071 cm^2) was pre-polished with different sizes of alumina powders over a polishing cloth and sonicated with water for 5 min, and dried at room temperature. The ink of the sample was prepared by dispersing -1.5 mg sample and 0.5 mg carbon black in 985 µl (1:1) isopropanol/water solution and 15 µl of 5% nafion solution. After obtaining homogeneous catalyst ink, 5 µl of it was drop casted over the GC electrode and dried at room temperature prior to electrochemical measurement.

Electrochemical measurement:

All the measurements were performed in a three-compartment electrochemical cell with a CHI 760D electrochemical workstation at room temperature in 1 M KOH (pH = 14) solution for OER. Linear sweep voltammetry (LSV) was measured at a scan rate of 5 mV/s. Hg/HgO and graphite rod were used as a reference electrode and a counter electrode for all the measurements, respectively. Potentials were calibrated with reversible hydrogen electrode (RHE) and adjusted by equation S1.

$$E_{RHE} = E°_{Hg/HgO} + 0.098 + 0.0591pH \quad \text{.....S1}$$

All the polarisation curves were presented here with iR compensated $(E\text{-}iR_s)$[3]; where i is the current and R_s is the uncompensated ohmic resistance derived from the impedance spectroscopy study. The correction was carried out to get the intrinsic electrocatalytic activity of the electrode by eliminating the electrolyte and catalyst resistance on electrochemical behavior. The Tafel plots were obtained from the polarization curves, and the slopes were calculated by linear fitting using equation S2.[4–7]

$$\eta = a + b \log j \quad \text{.....S2}$$

where η, a, b and j are the over potential, Tafel constant, Tafel slope, and current density, respectively. The over potential (η) was calculated by following equation S3.

$\eta = E\ (vs\ RHE) - 1.23\ V$……S3

The long-term durability of the sample was verified by modifying the sample ink on the well-polished GC plate using the chronopotentiometric technique. Faradaic double-layer capacitance (C_{dl}) and the electrochemical accessible surface area (ECSA) were measured from the cyclic voltammetric study at different scan rates (10 to 200 mVs^{-1}) in the non-faradaic region (1 to 1.1V) vs. RHE. Current linearly varies with the scan rate following equation S4.[8]

$i = \nu \times C_{dl}$……S4

By plotting the current differences (cathodic and anodic) with scan rate at 1.05 V vs. RHE, show a linear trend, and C_{dl} value can be evaluated from the slope (C_{dl}= slope/2). The ECSA is evaluated by the following equation S5.

$ECSA = C_{dl}/C_s$…….S5

where Cs is the specific capacitance of the catalyst. From the equation S5 its clear that, ECSA is directly prortional to the C_{dl} and the relative ECSA is used here for the interpretation by considering the ECSA value for ReS_2 NS as 1. The electrochemical impedance spectroscopy was measured in the 10^6 to 1 Hz frequency region at an over the potential of η = 1.524V vs. RHE. The mass activity (Ag^{-1}) of the catalyst was evaluated from the active catalyst loading ($mgcm^{-2}$) and the measured current density ($mAcm^{-2}$) at a constant overpotential of 300 mV following equation S6.

Mass activity = j/m……S6

Where, j is the current density ($mAcm^{-2}$), at an over potential (η), m is mass loading of the catalyst mg (0.1056 $mgcm^{-2}$).

The number of active sites and turn-over frequency (TOF) were calculated following the previously reported method.[9] First, cyclic voltammograms were recorded at a scan rate of 50 mVs^{-1} in the potential range of -0.2 to 0.6 V vs. RHE to calculate the number of active sites (n) on the materials in 1M phosphate buffer (pH=7.4). The value of n is calculated by using equation S7.[10]

$n = Q_{cv}/2F$……S7

where, Q_{cv} is the integrated charge derived from CV and F is the faraday constant, 96485 $Cmole^{-1}$. And the TOF number was calculated using the following equation S8. [11]

TOF = I/4Fn……S8

Where, I is the current in ampere (A).

Rotating Ring Disk Electrode (RRDE) experiments were carried out using a VSP-300 multi-channel potentiostat (Biologic Inc.), a rotator, GC Disk-Pt Ring of Pine instruments, USA. The O_2 bubbles generation at the disk electrode was verified by the oxygen reduction reaction (ORR) polarisation experiment at the ring electrode at a rate of 5 mVs^{-1} in 1M KOH at a fixed rotation speed of 1600 rpm by applying a constant potential of 1.5 V vs. RHE at the disk electrode. OER LSV polarization on the disk electrode was plotted. At the same time, the current response on the ring electrode was also measured. After applying a constant current at the disk electrode (I_d) for the oxygen generation, the current at the ring electrode (I_r) was measured. The Faradaic efficiency (FE) was measured following the equation S9.[12–14]

$$FE = \frac{I_r}{NI_d} \quad \text{……S9}$$

Where Ir and Id are the currents at ring and disk electrode, and N is the current collection efficiency of the Pt ring (N ~ 0.2).

Table S1: OER performance comparison of our $Ni_d(5)S_v@ReS_2$ NS sample with other reported catalysts.

Sl. No	Materials	Overpotential (mV) @ 10 mA/cm^2	Tafel slope (mV/dec)	Electrolyte	References
1.	Graphene@FeCoNi CuCr HEA	330	80	1 M NaOH	[15]
2.	CoS/MoS_2	280	79	1 M KOH	[16]
3.	Fe-doped NiS_2/MoS_2	280	56	1 M KOH	[17]
4.	Co@NC/NCNS	390 mV @η_{15}	82	0.1M KOH	[18]
5.	$Cu_2S/TiO_2/Cu_2S$	284	72	1M KOH	[19]
6.	CuNiS	337	43	1M KOH	[20]
7.	MoS_2 QD	370	39	1M KOH	[2]
8.	Ov-Hm	250	34	1M KOH	[12]
9.	Re/ReS_2-7H/CC	290	81	1M KOH	[21]
10.	$Ni_d(5)S_v@ReS_2$ NS	270	31	1M KOH	This work

Table S2: Comparison of different electrochemical parameters of the as-synthesized catalysts

Catalysts	Cdl ($\mu F/cm^2$)	ECSA	Mass Activity	TOF (s^{-1}) at 300 mV	R_s (Ω)	R_{ct} (Ω)	Tafel Slope (mV/dec)
$Ni_d(5)S_v@ReS_2$ NS	0.15	3.4	122	0.409	4.51	52.64	31
$Ni_d(5)@ReS_2$ NS	0.1	2.2	7.0	0.171	5.05	79.58	38
ReS_2 NS	0.044	1	3.4	0.113	5.65	570.6	53.5

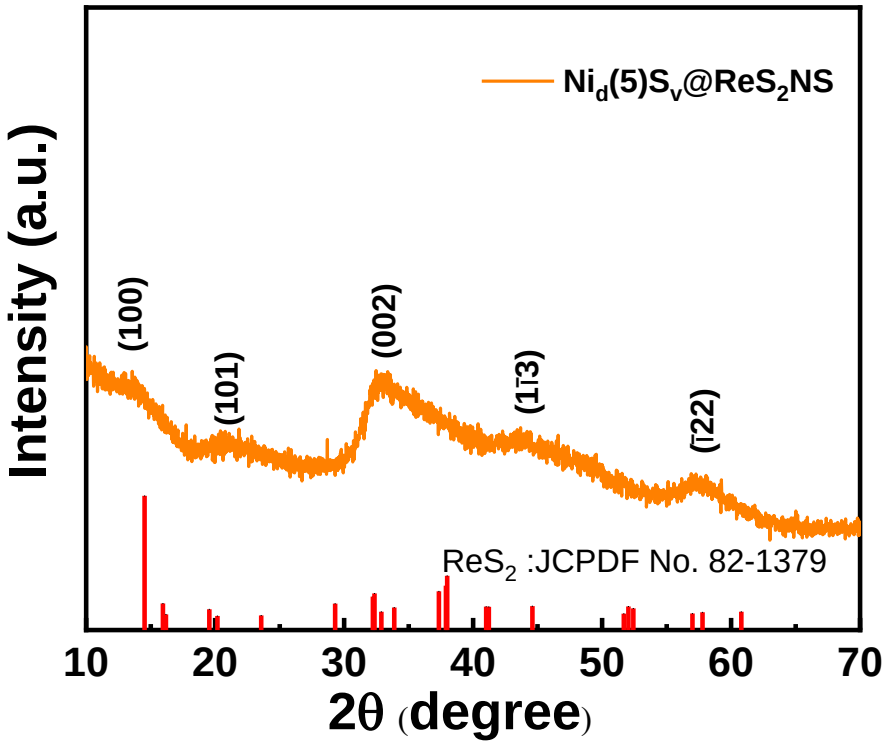

Fig. S1: XRD pattern of $Ni_d(5)S_v@ReS_2$ NS.

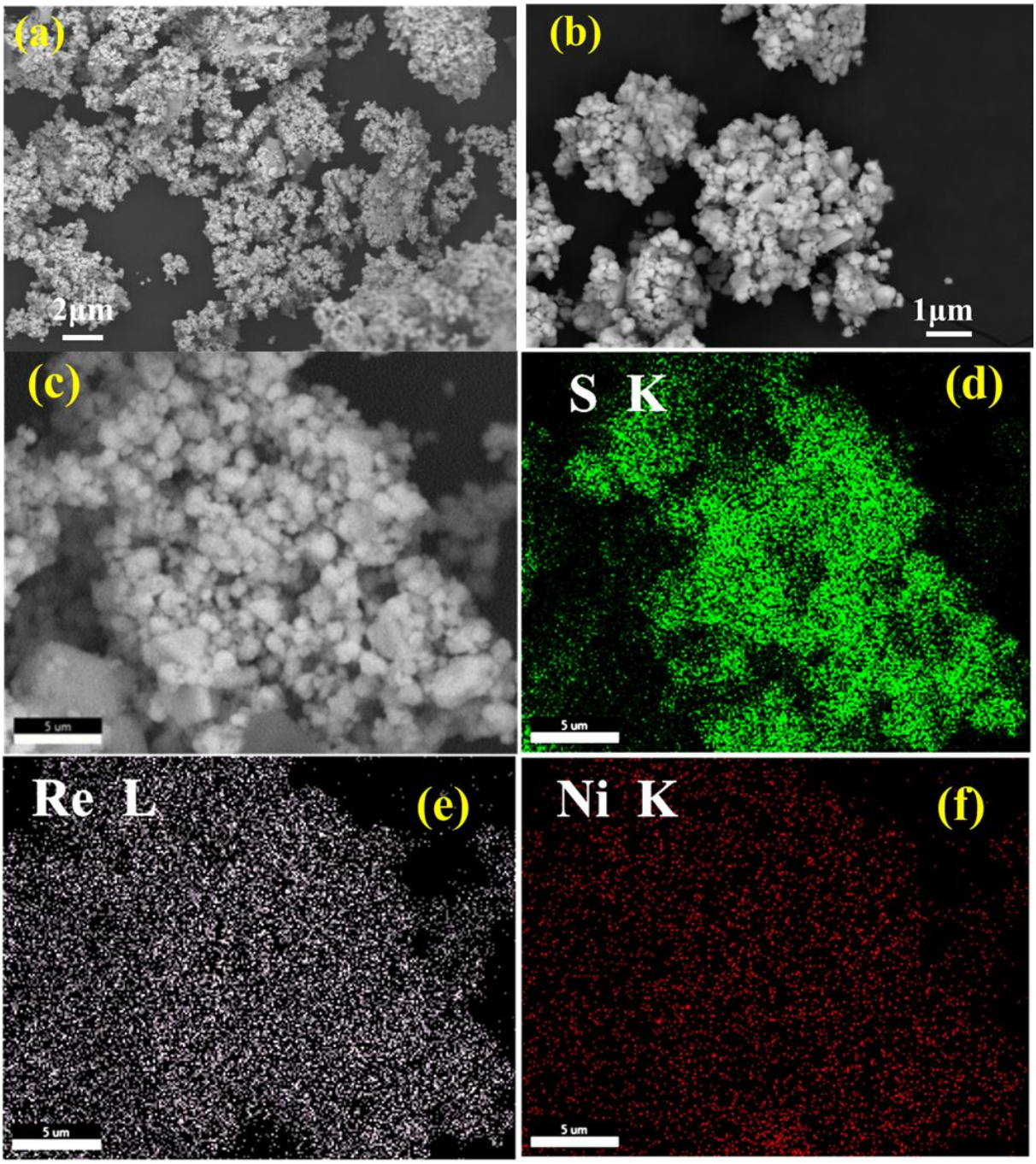

Fig. S2: SEM images (a-c) of the $Ni_d(5)S_v@ReS_2$ NS, and the elemental color mapping of the individual elements (S, Re and Ni).

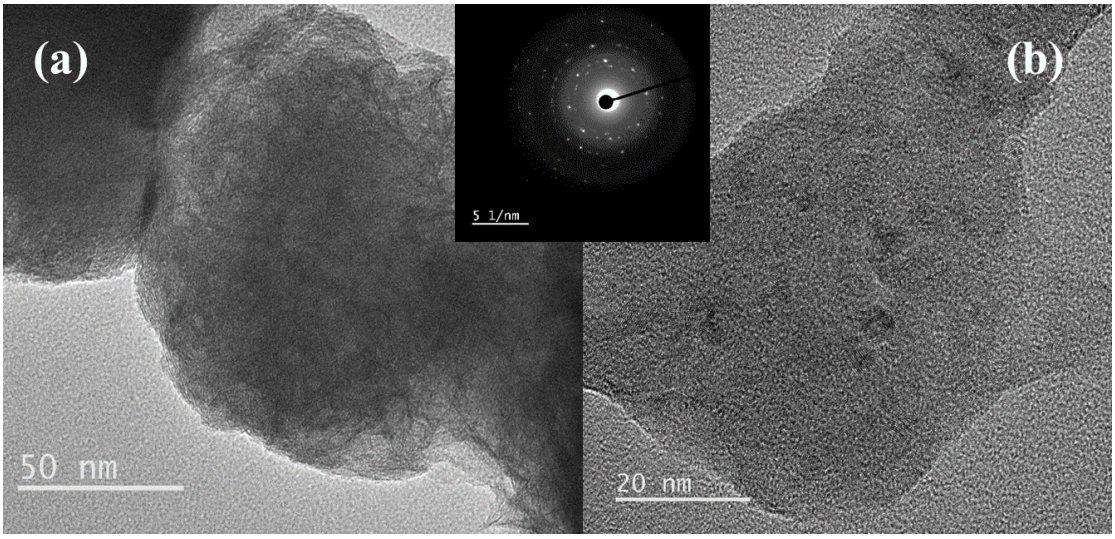

Fig. S3: TEM images (a & b) and SAED pattern (inset) of $Ni_d(5)S_v@ReS_2$ NS

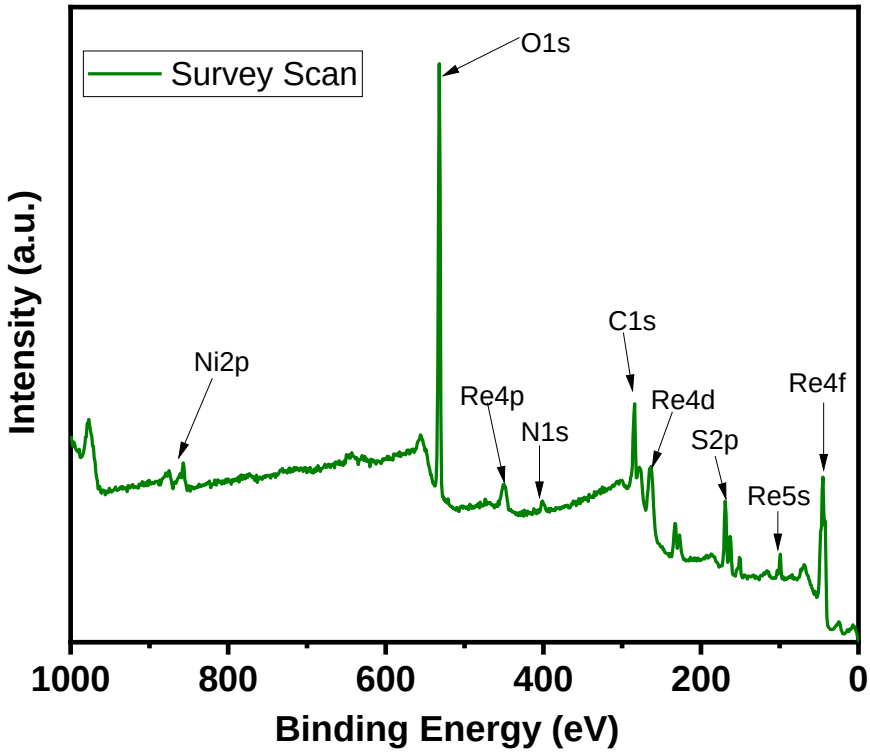

Fig. S4: Survey scan of the $Ni_d(5)S_v@ReS_2$ XPS spectra.

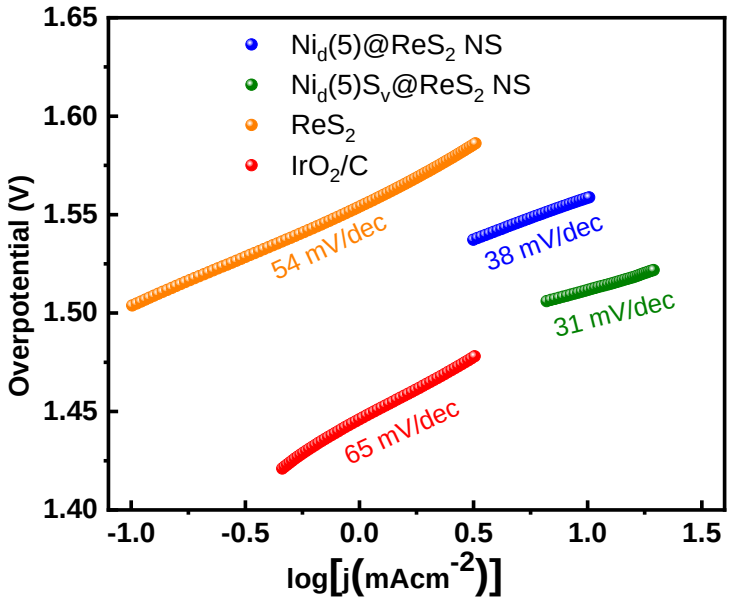

Fig. S5: Tafel plot of all the catalysts, $Ni_d(5)S_v@ReS_2$ NS, $Ni_d(5)@ReS_2$ NS, ReS_2 NS and IrO_2/C.

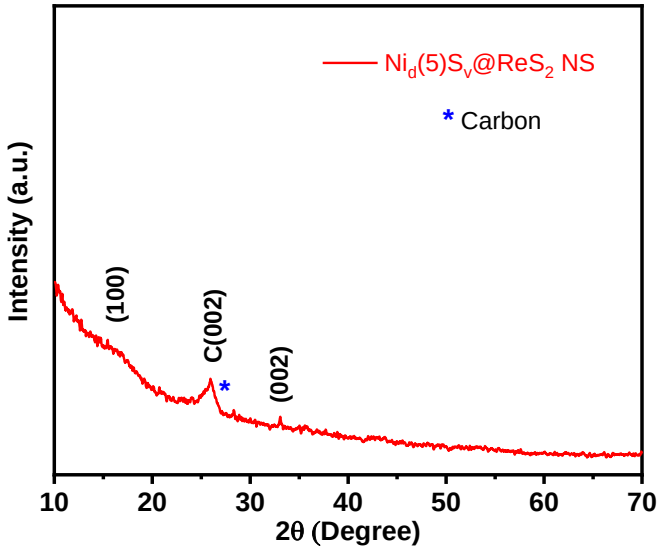

Fig. S6: XRD pattern of the Ni_dS_v@ReS_2 NS after long term stability study. Carbon peak comes from the, additive graphitic carbon added while making the ink for electrochemical study, so the other peak intensity appears to be very low.

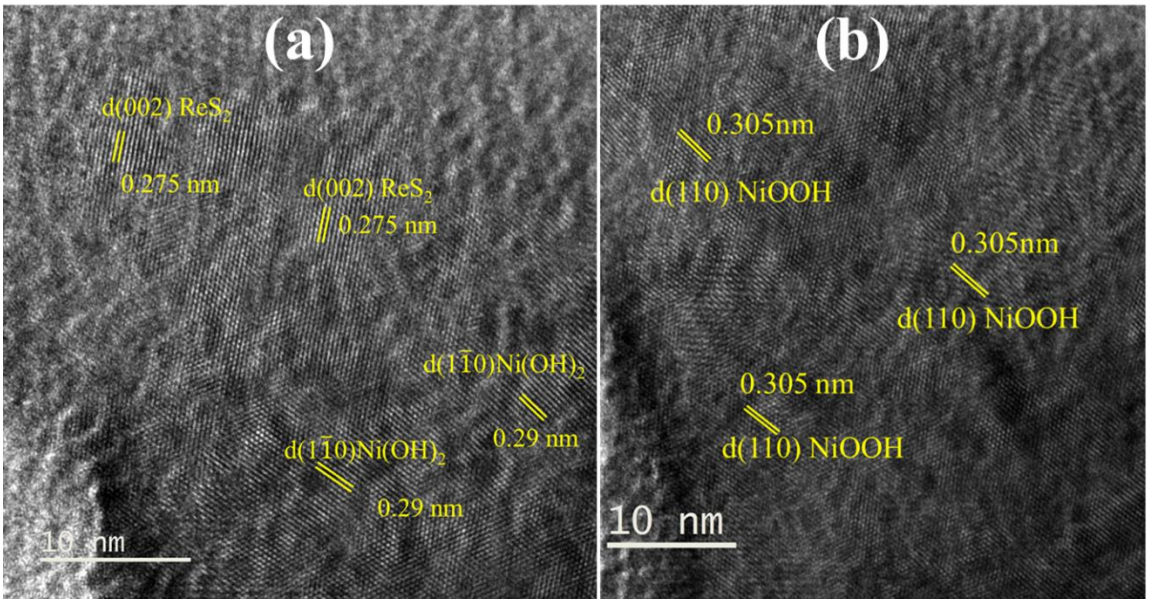

Fig. S7: HRTEM images (a & b) of the catalyst Ni_dS_v@ReS_2 NS after long-term stability study.

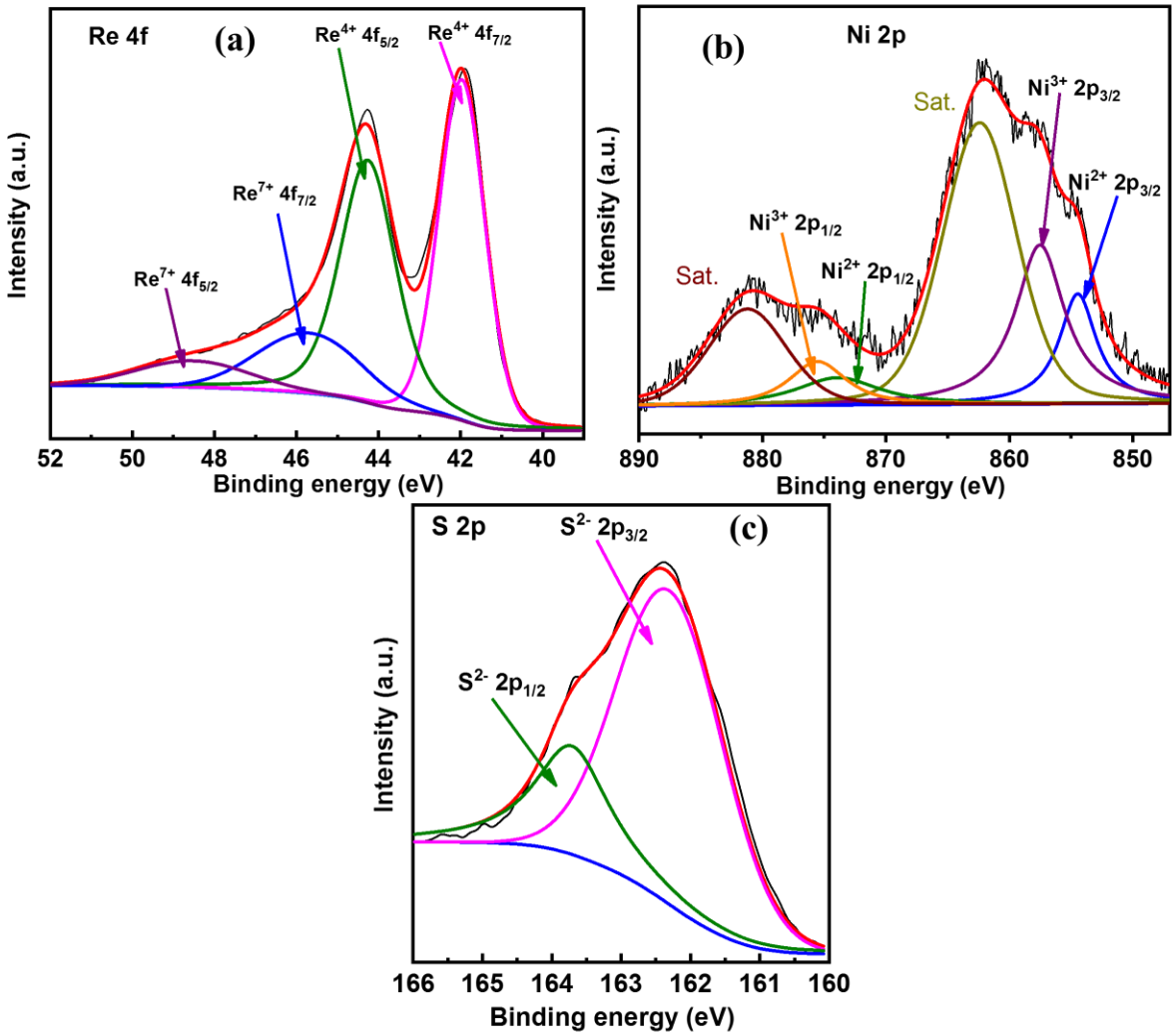

Fig. S8: Fine XPS spectra of Re 4f (a), Ni 2p(b), and S 2p (c) of the catalyst Ni_dS_v@ReS_2 NS after long-term stability study.

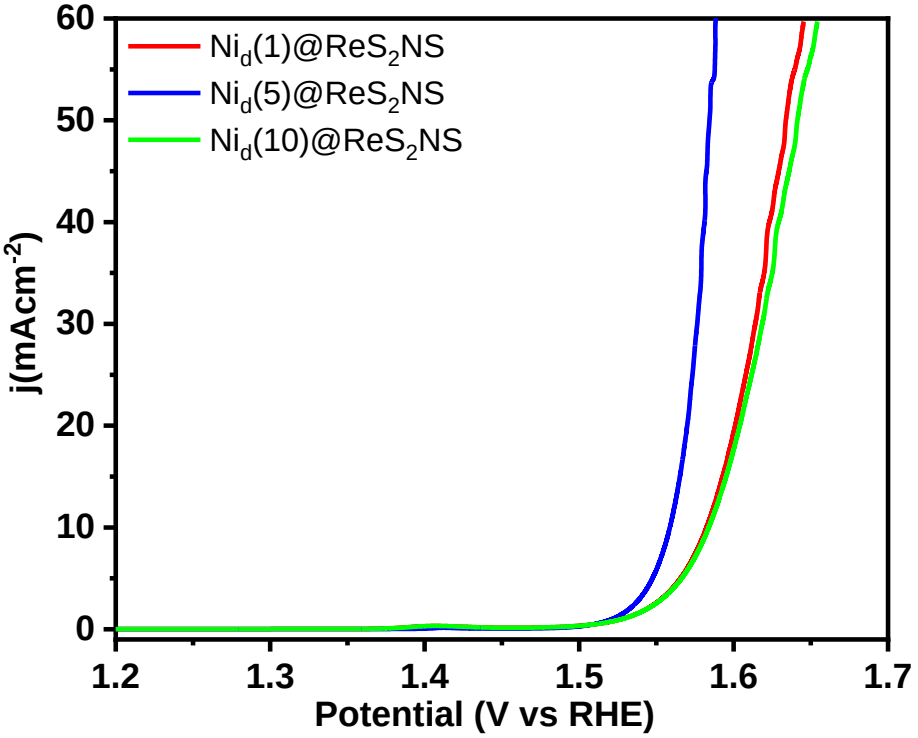

Fig. S9: OER LSV polarization plots of different % of Ni doped ReS_2 NS

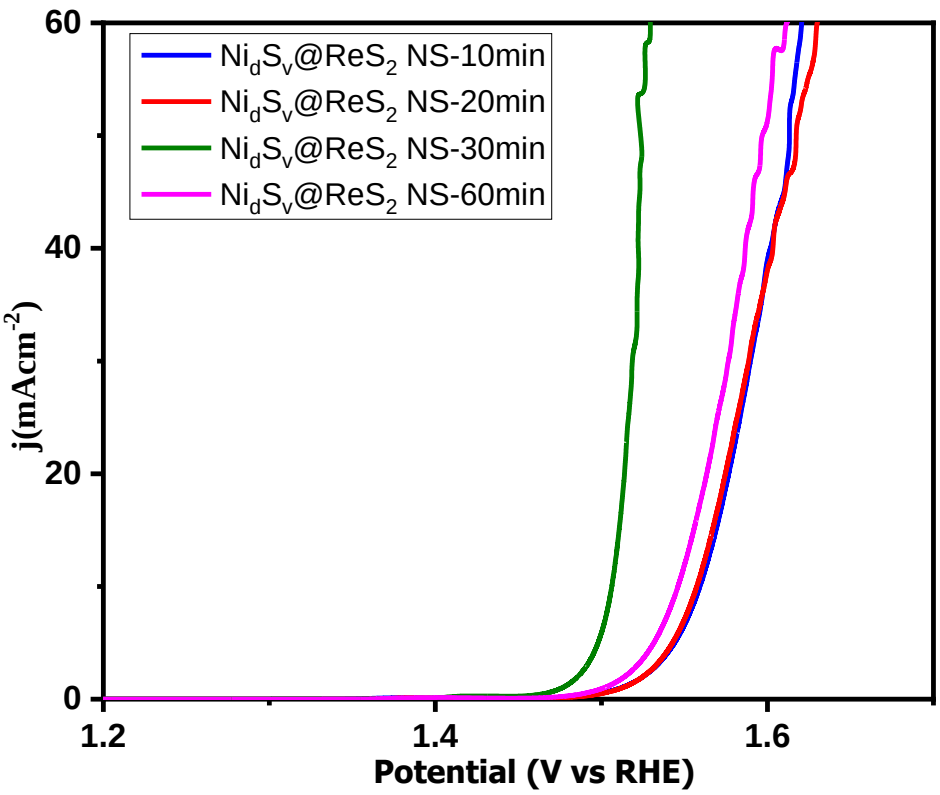

Fig. S10: OER LSV polarization curves of $Ni_d(5)S_v@ReS_2$ NS with different S vacancy time

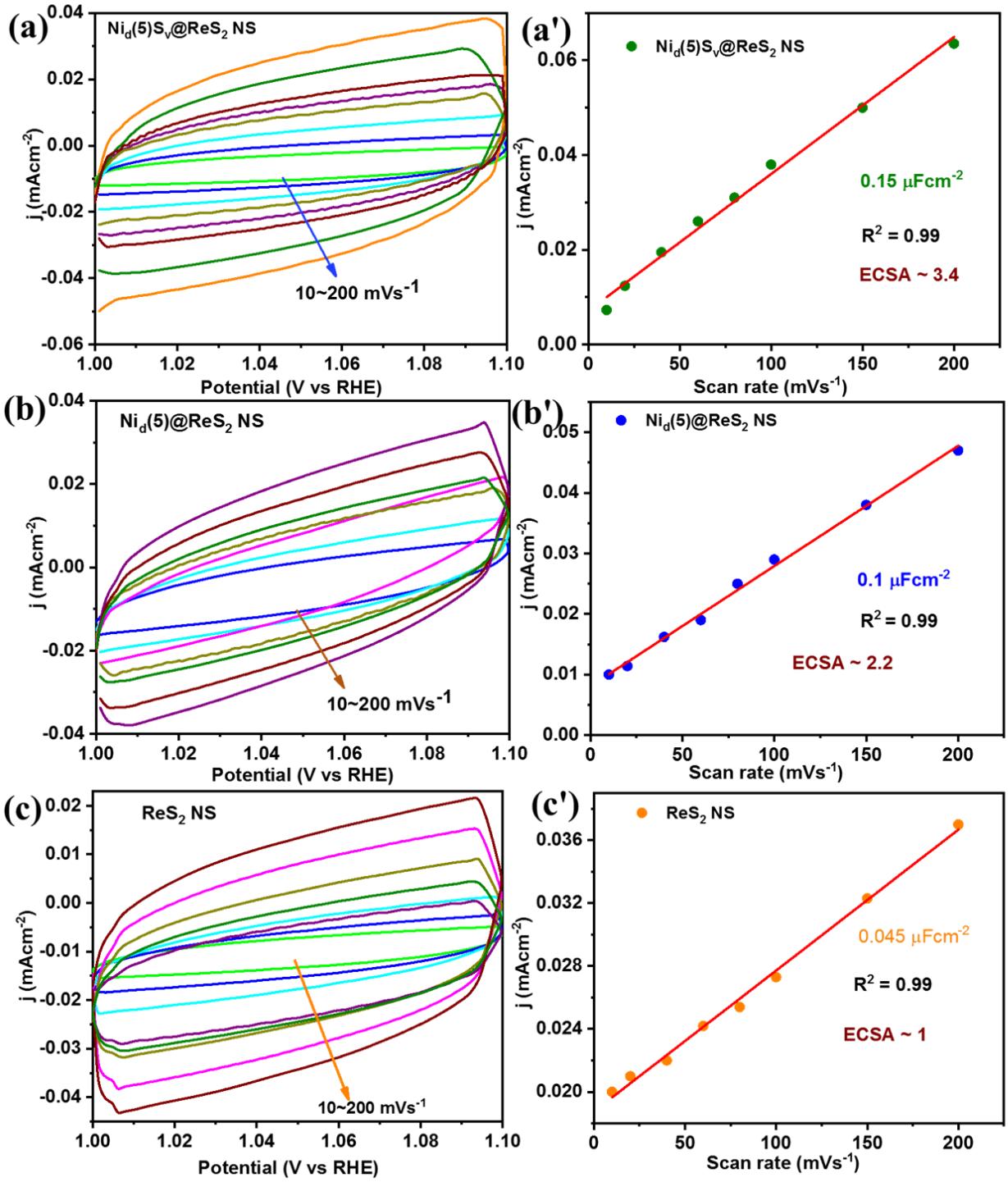

Fig. S11: Cyclic voltammograms obtained from the non-Faradic region of as-synthesized ReS_2 NS, $Ni_d(5)@ReS_2$ NS, and $Ni_d(5)S_v@ReS_2$ NS catalyst at different scan rates. The corresponding fitted plot of scan rate vs. the anodic and cathodic current difference measured at 1.05V.

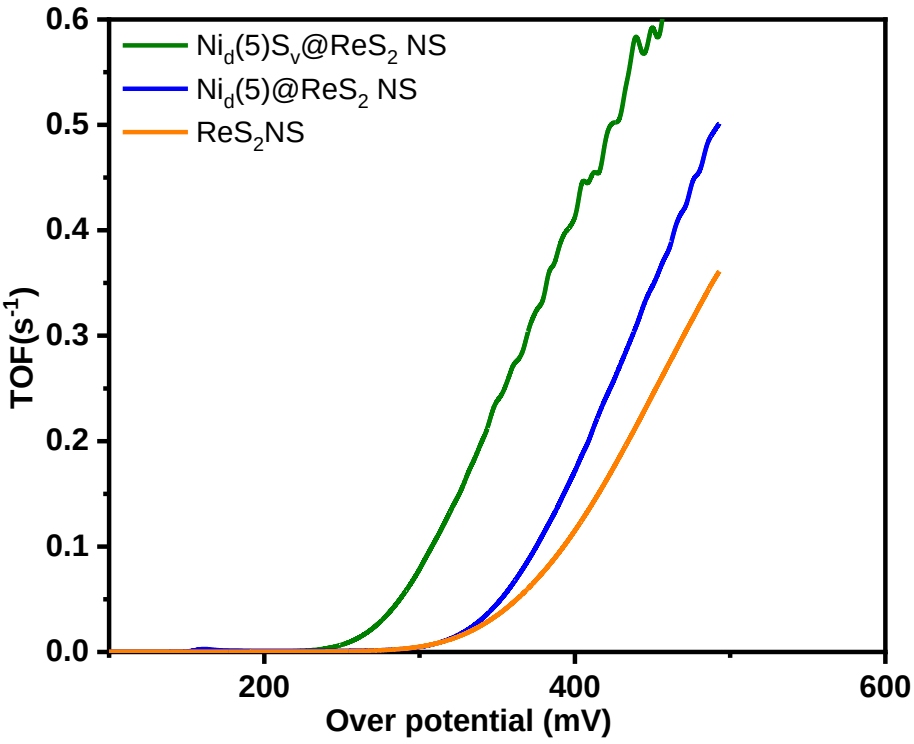

Fig. S12: TOF plot of different as-synthesized ReS_2 NS, $Ni_d(5)@ReS_2$ NS and $Ni_d(5)S_v@ReS_2$ NS catalysts towards OER.

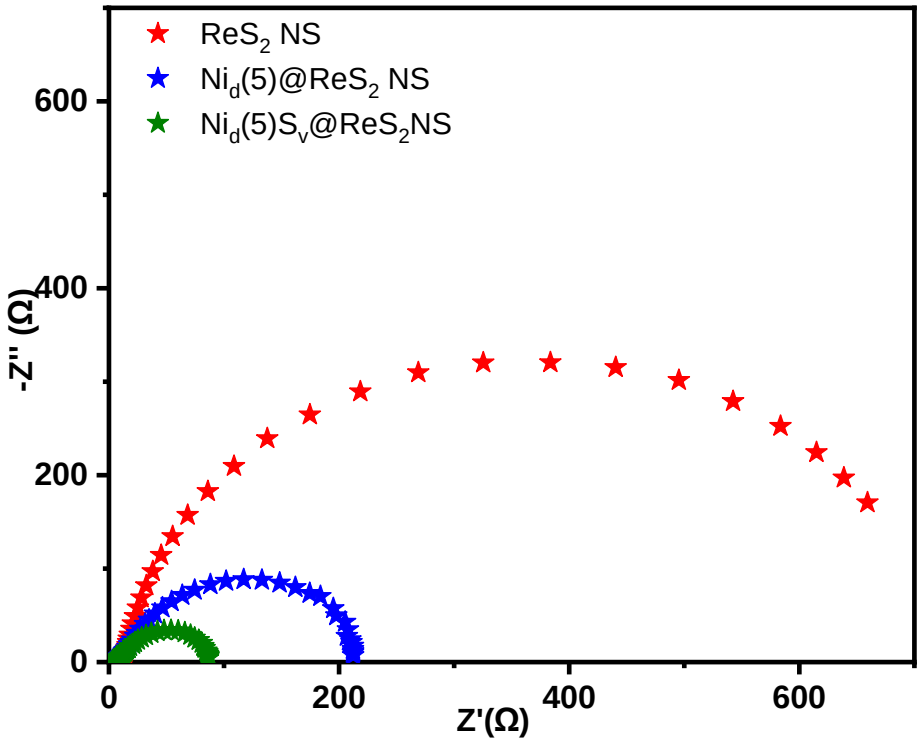

Fig. S13: Nyquist impedance spectra of the as-synthesized ReS_2 NS, $Ni_d(5)@ReS_2$ NS and $Ni_d(5)S_v@ReS_2$ NS catalysts.

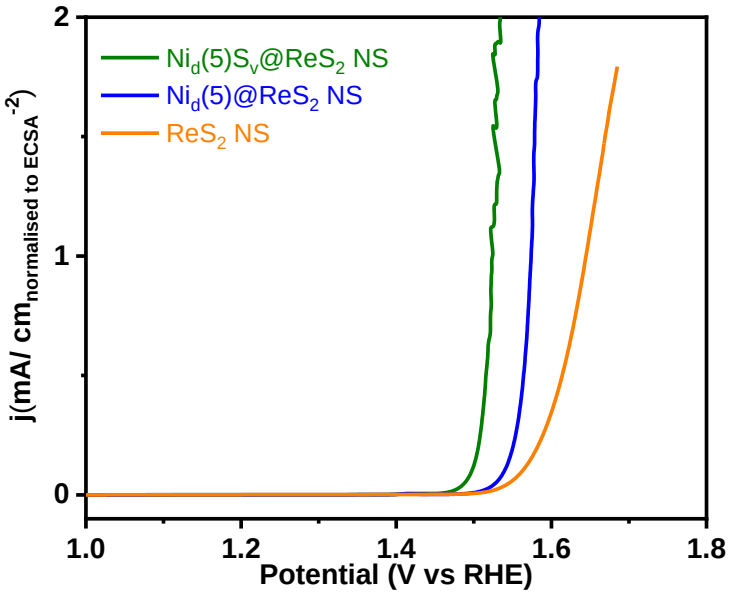

Fig. S14: LSV plots of the catalysts where current density are normalized with ECSA values.

Elemental dissolution study

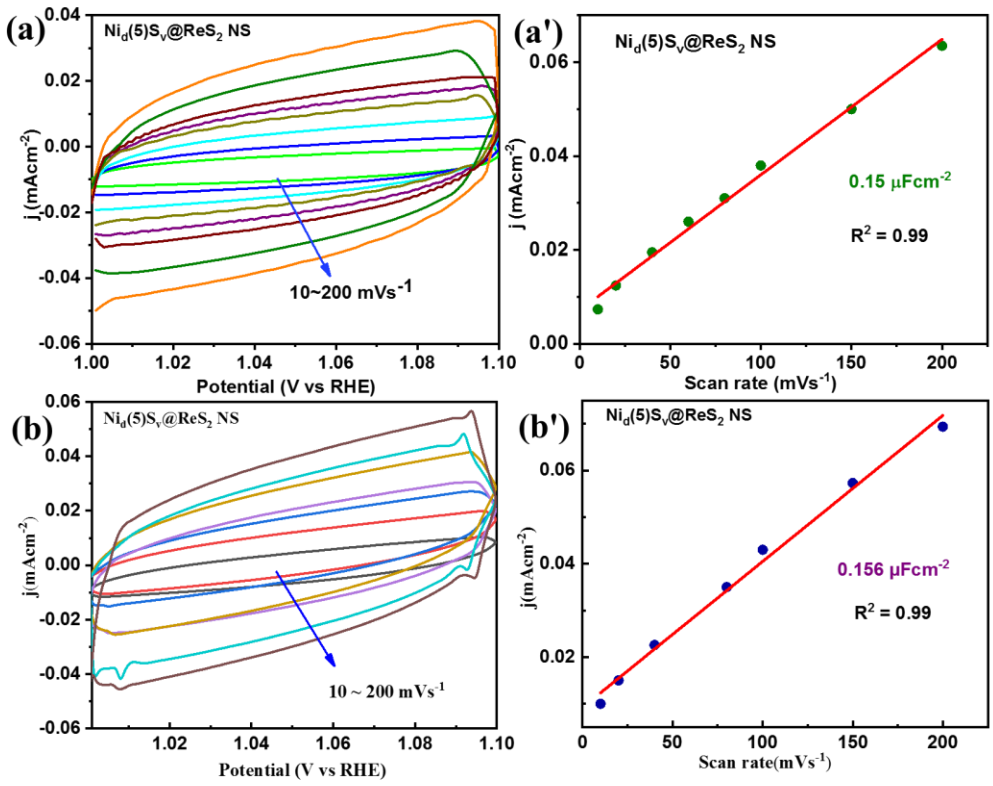

Fig. S15: Cyclic voltammograms at different scan rates obtained from the non-Faradic region of as-synthesized Ni$_d$(5)S$_v$@ReS$_2$ NS catalyst (a) before (b) after long term stability study. The corresponding fitted plot of scan rate vs the anodic and cathodic current difference measured at 1.05V for as synthesized catalysts (a', b').

There is no such significant change on C_{dl} before stability (0.15 μFcm^{-2}) and after stability (0.156 μFcm^{-2}) observed. It signifies three is no such elemental dissolution occurs on Ni$_d$(5)S$_v$@ReS$_2$ NS during long-term stability test.

However, the elemental dissolution study on the electrolyte after long-term stability was further analysed by ICP-OES measurement. It was found that there is very low concentration (~1.2 ppm) of the Re was found in the electrolyte, whereas no concentration of Ni was observed. The very small dissolution of Re may be due to the presence of loosely bound impurities of Re precursor, ReO_4^- (Re^{7+}) on the catalyst. That has been evidenced from the XPS analysis after the stability study. The XPS peak of Re^{7+} is significantly decreased (Fig. 2b and Fig. S8a). It signifies that the as-prepared catalyst is stable.

References:

1 B. Mohanty, B. K. Jena, M. Kandasamy, N. Dalai, R. K. Sahu, R. M. Kadam, B. Chakraborty and B. Jena, *Sustain. Energy Fuels*, 2020, **4**, 3058–3065.

2 B. Mohanty, M. Ghorbani-Asl, S. Kretschmer, A. Ghosh, P. Guha, S. K. Panda, B. Jena, A. V. Krasheninnikov and B. K. Jena, *ACS Catal.*, 2018, **8**, 1683–1689.

3 M. Mathankumar, K. Karthick, A. K. Nanda Kumar, S. Kundu and S. Balasubramanian, *ACS Sustain. Chem. Eng.*, 2021, **9**, 14744–14755.

4 U. Kayal, B. Mohanty, P. Bhanja, S. Chatterjee, D. Chandra, M. Hara, B. Kumar Jena and A. Bhaumik, *Dalt. Trans.*, 2019, **48**, 2220–2227.

5 P. V. Shinde, D. S. Gavali, R. Thapa, M. K. Singh and C. S. Rout, *AIP Adv.*, 2021, **11**, 105010.

6 S. Chakrabartty, S. Karmakar and C. R. Raj, *ACS Appl. Nano Mater.*, 2020, **3**, 11326–11334.

7 S. Shit, S. Bolar, N. C. Murmu and T. Kuila, *Chem. Eng. J.*, 2021, **417**, 129333.

8 C. Xia, Q. Jiang, C. Zhao, M. N. Hedhili, H. N. Alshareef, C. Xia, Q. Jiang, C. Zhao, M. N. N. Hedhili and E. Alshareef, *Adv. Mater.*, 2016, **28**, 77–85.

9 S. Kamila, B. Mohanty, A. K. Samantara, P. Guha, A. Ghosh, B. Jena, P. V. Satyam, B. K. Mishra and B. K. Jena, *Sci. Reports 2017 71*, 2017, **7**, 1–13.

10 D. Merki, S. Fierro, H. Vrubel and X. Hu, *Chem. Sci.*, 2011, **2**, 1262–1267.

11 M. R. Gao, X. Cao, Q. Gao, Y. F. Xu, Y. R. Zheng, J. Jiang and S. H. Yu, *ACS Nano*, 2014, **8**, 3970–3978.

12 B. Mohanty, Y. Wei, M. Ghorbani-Asl, A. V. Krasheninnikov, P. Rajput and B. K. Jena, *J. Mater. Chem. A*, 2020, **8**, 6709–6716.

13 S. Zhao, Y. Wang, J. Dong, C. T. He, H. Yin, P. An, K. Zhao, X. Zhang, C. Gao, L. Zhang, J. Lv, J. Wang, J. Zhang, A. M. Khattak, N. A. Khan, Z. Wei, J. Zhang, S. Liu, H. Zhao and Z. Tang, *Nat. Energy*, 2016 **1**, 16184.

14 Y. Yao, S. Hu, W. Chen, Z. Q. Huang, W. Wei, T. Yao, R. Liu, K. Zang, X. Wang, G. Wu, W. Yuan, T. Yuan, B. Zhu, W. Liu, Z. Li, D. He, Z. Xue, Y. Wang, X. Zheng, J. Dong, C. R. Chang, Y. Chen, X. Hong, J. Luo, S. Wei, W. X. Li, P. Strasser, Y. Wu and Y. Li, *Nat. Catal.*, 2019, **2**, 304–313.

15 R. Nandan, M. Y. Rekha, H. R. Devi, C. Srivastava and K. K. Nanda, *Chem. Commun.*, 2021, **57**, 611–614.

16 W. H. Huang, X. M. Li, X. F. Yang, H. Bin Zhang, F. Wang and J. Zhang, *Chem. Commun.*, 2021, **57**, 4847–4850.

17 J. Tian, X. Xing, Y. Sun, X. Zhang, Z.-G. Li, M. Yang and G. Zhang, *Chem. Commun.*, 2022,**58,** 557-560

18 Y. Wang, H. Yuan, F. Liu, T. Hu, R. Li, / Chemcomm and C. Communication, *Chem. Commun.*, 2021, **57**, 2994–2997.

19 S. Deng, Y. Shen, D. Xie, Y. Lu, X. Yu, L. Yang, X. Wang, X. Xia and J. Tu, *J. Energy Chem.*, 2019, **39**, 61–67.

20 D. Chinnadurai, R. Rajendiran and P. Kandasamy, *J. Colloid Interface Sci.*, 2022, **606**, 101–112.

21 Q.-Q. Pang, Z.-L. Niu, S.-S. Yi, S. Zhang, Z.-Y. Liu, X.-Z. Yue, Q.-Q. Pang, Z.-L. Niu, S.-S. Yi, Z.-Y. Liu, X.-Z. Yue and S. Zhang, *Small*, 2020, **16**, 2003007.